Author's Accepted Manuscript

Evolution of plasticity-based wear damage in gross sliding fretting of a Ti-6Al-4V non-conforming contact

A.L. Mohd Tobi, W. Sun, P.H. Shipway

TRIBOLOGY INTERNATIONAL

Editor: Philippa Cann

Cite this article as: A.L. Mohd Tobi, W. Sun and P.H. Shipway, Evolution of plasticity-based wear damage in gross sliding fretting of a Ti-6Al-4V non conforming contact, *Tribiology International* http://dx.doi.org/10.1016/j.triboint.2017.01.010

This is a PDF file of an unedited manuscript that has been accepted for publication. As a service to our customers we are providing this early version of the manuscript. The manuscript will undergo copyediting, typesetting, and review of the resulting galley proof before it is published in its final citable form. Please note that during the production process errors may be discovered which could affect the content, and all legal disclaimers that apply to the journal pertain.

Evolution of plasticity-based wear damage in gross sliding fretting of a Ti-6Al-4V non-conforming contact

A.L. Mohd Tobi[a,b*], W. Sun[b], P.H. Shipway[b]

[a]Structural and Integrity Monitoring Research Group, Faculty of Mechanical and Manufacturing Engineering, Universiti Tun Hussein Onn Malaysia, Batu Pahat, Malaysia.
[b]Faculty of Engineering, University of Nottingham, University Park, Nottingham, NG7 2RD, UK.

[*]abdlatif@uthm.edu.my

Abstract

This paper examines the evidence for a plasticity based wear mechanism in the fretting wear of Ti-6Al-4V. Driven by near-surface plastic strain accumulation, the generation of wear debris evolves from coarse metallic debris towards loose fine oxide debris generating *W*-shape wear scar. The overall wear effect however, is less pronounced at the later stages of wear due to a reduced propensity for plastic deformation in the contact associated with wear induced contact pressure reduction. The evidence suggests that the high wear rate at the early stages of a fretting test are due to debris generation associated with gross plasticity whilst at the later stages, lower wear is associated with less plasticity accumulation.

Keywords: plasticity wear; gross sliding, fretting wear; Ti-6Al-4V.

1. Introduction

Fretting is a mechanical contact problem associated with small-scale displacements between contacting surfaces and may result in wear and fatigue. Problems have been observed in a variety of contexts such as aeroengine spline shaft couplings, aeroengine turbine blade and heat exchanger pipe and support contacts [1 – 3]. The small cyclic relative displacement of contact surfaces associated with fretting ranges from few nanometers to few micrometers [4]. The contact surfaces also being subjected to some loading conditions (normal and/or fatigue loading) [5 – 7].

It is generally accepted that the main variables that dictate the damage behaviour in fretting are the applied normal load, the contact relative displacement, and the coefficient of friction (COF) between the surfaces [8 & 9]. Fretting in the stick regime occurs when the total imposed displacement is predominantly accommodated by the elastic deformation of the contacting bodies and there is no slip between the contacting surfaces; fatigue crack formation can be observed in such cases. Partial slip takes place when the contact region is made up of both a zone which is slipping and a zone which is stuck (i.e. not slipping); here, damage is associated with a reduction in fatigue life. In gross sliding, slip occurs across the whole contact region. The main damage mechanism in this case is fretting wear which is characterised by material removal from the surface assisted by oxidation, but with limited crack formation [10]. In general, high loads with low applied displacement leads to partial slip fretting which is associated with fatigue, whereas low load and high displacement conditions promote the gross sliding fretting which is mainly associated with wear. This behaviour has been described by running condition fretting maps and damage mechanism fretting maps [11 – 13].

One of the most common and frequently cited relationships for sliding wear is associated with Archard's wear model [14]. The relationship is based on experimental work from the early 1950s which suggests that for sliding between two surfaces, stable wear behaviour can be described by the following equation [15];

$$\frac{V}{S} = K\frac{P}{H} \quad (1)$$

where V is the total wear volume, S is the sliding distance, K is the (dimensionless) wear coefficient, P is the normal load and H is the hardness of the softer material in the sliding couple.

Fouvry et al. [16 - 18] proposed the concept of wear based upon the energy dissipated in overcoming friction when the fretting contact slides. Using the concept of the fretting loop (a force-displacement trace for the fretting cycle), they calculated the total accumulated dissipated energy throughout the sliding period and showed that it is directly proportional to the wear volume with the dimensional constant of proportionality being termed "the energy wear coefficient". Another important aspect is a term called the "energy threshold"; this is the energy required to be dissipated when wear is observed to commence (i.e. material is lost from the contact) [16 & 17].

While Archard's wear model is based upon the concept of plastic deformation of asperities, in fretting a more significant plasticity accumulation (termed the ploughing effect) does contributes significantly to wear [10 & 19]. It has been reported by Fouvry et al. [20] that a contact which exhibits a high COF does experience higher rates of wear under the same loading conditions. Moreover, as well as the materials types, the wear debris itself plays a role in the overall rate of wear in the contact, both in the kinetics of its formation and its retention in (or egress from) the contact [21 & 22].

The generation of wear debris in fretting takes place due to particle detachment associated with adhesion, abrasion, corrosion and asperity fatigue [12]. Hurricks [23] characterised the fretting wear process into three stages, as follows;

(i) During the initial stage of fretting, the disruption of the natural oxide surface layers on the metal results in metal-to-metal contact. This leads to adhesion and metal transfer and subsequently, to local welding and roughening of the surface.

(ii) The next stage is associated with debris formation which results from oxidation of fretted metal during the wear process. Abrasive wear may then occur if the oxidised debris is harder than the metal surface.

(iii) In the final steady state stage, the accumulated debris forms a compacted debris bed and reduces the abrasive wear process by protecting the contacting surfaces due to the load carrying capacity of the compacted debris.

Models for the initiation of a tribologically transformed structure (TTS) based on accumulation of plastic hardening in fretting wear have been presented in [24 & 25]. Fouvry et al. [20] have argued that wear damage relies on the elastic-plastic shakedown response of materials, and suggested that the high wear regime in fretting is due to the occurrence of global surface shear plasticity, while the low wear regime is governed by local asperity plasticity (Fig. 1). Kapoor [26] presented the concept of ratchetting wear in sliding contacts. He suggested that the accumulation of plasticity by ratchetting leads to ductility exhaustion and thus cracks are induced parallel to the surface, leading to delamination wear. A plasticity-assisted oxidation model was proposed by Everitt et al. [27] to describe the wear process of Ti-6Al-4V fretting contact.
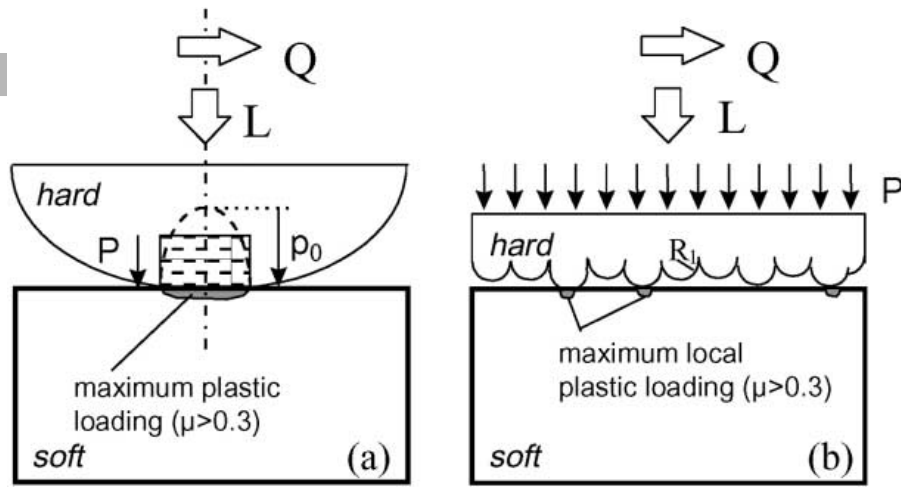
Fig. 1. Schematic view of plasticity initiation for a) gross plasticity, b) asperity based plasticity, after [20].

This paper will investigate the evidence for plastic deformation which leads to the generation of wear in fretting. The mechanism for the development and accumulation of plastic deformation in fretting is investigated and related to the concept of plasticity driven wear. The effect of two different regimes of loading on the fretting wear is quantified and its significance in plasticity induced wear is studied. The effect of plastic deformation associated with the shear yielding associated with high contact pressures is also discussed for the two loading conditions.

2.   Experimental procedure

The material investigated in this study is Ti–6Al–4V, which is widely used in aeronautical applications. Ti–6Al–4V is an α + β alloy; the α phase is a hexagonal close-packed (HCP) phase whilst the β phase is a body-centred cubic (BCC) phase. The specimen pair was assembled in a cylinder-on-flat configuration as shown in Fig. 2. The flat specimens have a length of 44 mm, a width, w of 10 mm and a thickness, t of 6 mm. The round specimens are also 44 mm long and the radius of the cylindrical specimen, R is 6 mm. The alloy has a measured hardness of HV(0.3) of 350–370.

The flat specimen is mounted on the lower specimen mounting block (LSMB), which is stationary, and the cylindrical specimen is mounted on the upper specimen mounting block (USMB). The USMB was loaded through a dead weight configuration and the normal load that resulted is termed P; normal loads of 500 N and 1000 N were employed in this programme of work. The main components in the rig used for the fretting experiments are illustrated in Fig. 3. The motion of the USMB (and hence the cylindrical specimen) is created by a sinusoidally varying force generated by an electromagnetic vibrator (EMV). The displacement of the USMB is monitored by a capacitance displacement sensor which is mounted to the LSMB and is recorded throughout the duration of the test.

The EMV was controlled to achieve displacement amplitude, Δ, of 120 μm with a fretting frequency of 20 Hz. The tangential force, Q, is measured and recorded throughout the entire test by a piezoelectric load cell which is connected to the quasi-stationary LSMB. The LSMB is mounted on flexures which provide flexibility in the horizontal direction so that the majority of the tangential force is transmitted through the much stiffer load path which contains the load cell as shown in Fig. 3. Both displacement and load sensors have been calibrated (both externally and in situ) in static conditions. The load and displacement signals are sampled at a rate of 200 measurements per fretting cycle.

The behaviour of the contact can be monitored throughout the test by examination of the fretting loops; a fretting loop is a plot of a cycle of the measured tangential force as a function of the displacement. All experiments were carried out in the gross sliding regime (slip occurs across the entire contact). Gross sliding was maintained throughout the test by ensuring that the load conditions were chosen so that the fretting loop exhibited a quadrilateral shape. The displacement of the USMB is

measured, but it must be noted that this is not the same as the slip in the contact; there are components with compliance which physically separate the contact from the point of measurement, and hence the measured displacement amplitude is always slightly larger than the contact slip amplitude. The effects of normal load and number of fretting cycles on the wear damage were investigated at different test durations. Table 1 shows the test matrix that has been followed for the test programme.
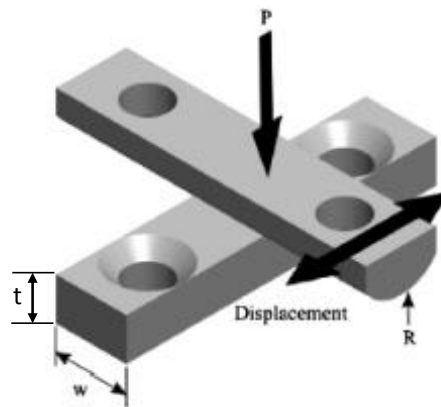

Fig. 2. Schematic arrangement of the crossed cylinder-on-flat fretting experiment. w = 10 mm, R = 6 mm and P = 500 N or 1000 N.
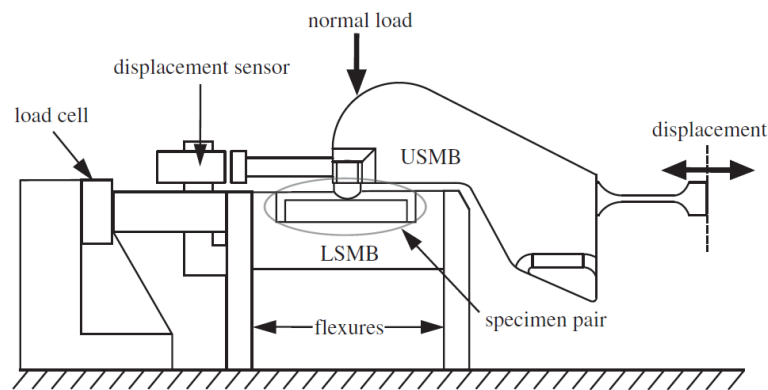
Fig. 3. Illustration of the main components of the fretting apparatus used in this study.

Table 1. Conditions of fretting tests.

Normal Load, P (N)	500, 1000
Applied displacement amplitude, Δ (μm)	120
Duration, N (number of cycles)	1,250-20,000
Frequency (Hz)	20
Room temperature (^{o}C)	20.0-24.0
Relative humidity (%)	30.0-35.0

After the completion of a fretting experiment, the specimens were blown with compressed air to remove loose debris, thus leaving any debris that was adhered to the specimen. To evaluate their topography, the wear scars on both the flat and cylindrical specimens were scanned using a Bruker Contour GT-I interferometer, which has a vertical resolution of approximately 0.15 nm and a lateral resolution of 4 μm. The scan areas on the flat and cylindrical specimens were 4 mm in width and 6 mm in length.
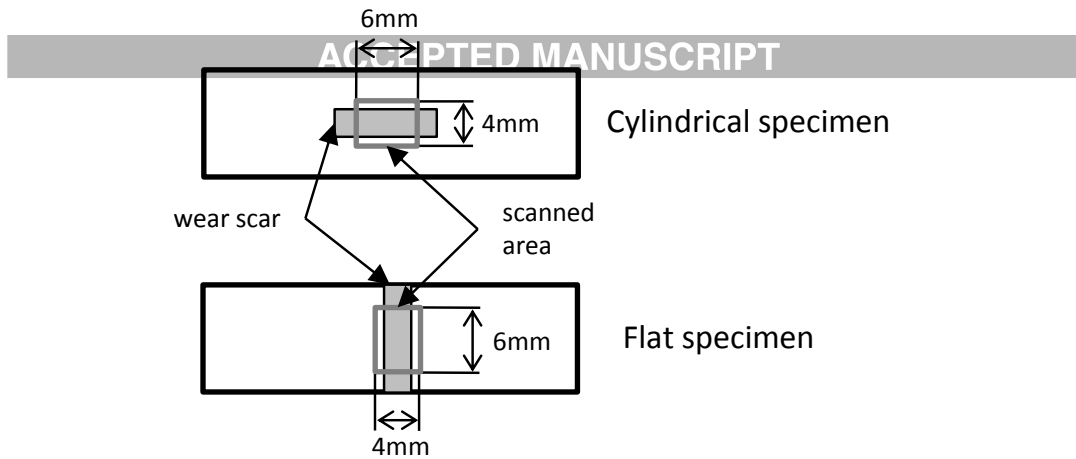
4

Fig. 4. Illustration of the areas profiled on both the flat and cylindrical fretting specimens.

The volume below each reference surface was regarded as the wear volume (V− Flat and V− Cyl for the flat and cylindrical specimens, respectively) and the volume of material above these surfaces was regarded as transferred volume (V+ Flat and V+ Cyl for the flat and cylindrical specimens, respectively). The total wear and transfer volumes for the couple (V− and V+, respectively) are defined as the sum of the respective volumes for the flat and cylindrical specimens for the scanned area (Fig. 5). The volume then extrapolated linearly to 10 mm contact width to take in to account overall wear volume of the wear scar.
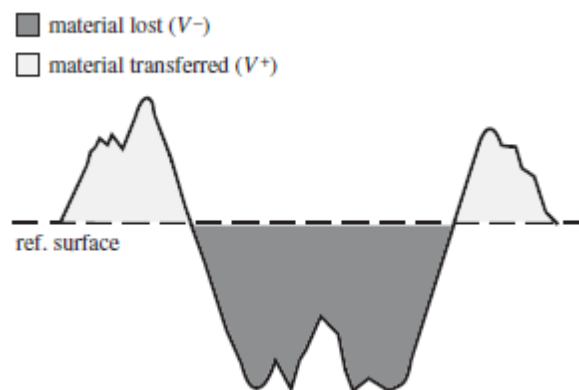
Fig. 5. Illustrations of the definition of wear and transfer volumes in a fretting scar.

Optical microscopy (Nikon ECLIPSE LV100ND with NIS-Elements imaging software v4.10.00) was initially used to take plan view and cross-sections images of the wear scars. These images give a general overview of the wear damage that has occurred by showing the width of the wear scar. Post-test examination of the cross-sections of wear scars on the flat specimens only was carried out by scanning electron microscopy (SEM) using a Philips XL30 scanning electron microscope to identify the wear and damage mechanisms operating. Backscattered electron (BSE) imaging was used to distinguish oxide from metallic material, as oxide (which is generally a main constituent of the debris which forms in the wear scar) has a lower average atomic number, resulting in a lower brightness in BSE imaging than the titanium. Energy dispersive X-ray (EDX) analyses were carried out to characterise the relative weightings of the elements such as oxygen, titanium, aluminium and vanadium in various regions of the damaged material.

Cross sections through the specimens were used to investigate the structure of the debris beds as well as to characterize any subsurface damage. Sections were taken from the flat specimen (through an area of interest identified by top

5

surface BSE images or profilometry) and then mounted in a conductive phenolic mounting resin. Once mounted, the section was ground using different grades of silicon carbide grinding paper down to P4000 (5 μm) before finally being chemical–mechanical polished down to 0.1 μm using an MD-CHEM colloidal silica (Struers). To reveal microstructural features in the cross sections, specimens were etched using Kroll's Reagent (consisting of 2 ml of hydrofluoric acid, 5 ml nitric acid and 97 ml water) for ~ 10 seconds. Using cross-sections, the make-up of the third body layers and subsurface deformation was examined. EDX analysis was conducted to confirm the chemical composition of the third body layer formed during the fretting tests and any chemical changes within the Ti-6Al-4V itself.

3. Experimental results

Fretting test loops are shown in Fig. 6. The plots are constructed from the measured tangential force against the measured applied displacement of the fretting contact. The tangential force arises from a combination of sliding friction and from geometrical changes which either promote or resist motion. Both cases show almost parellogram shaped loops, suggesting gross sliding fretting. It can also be observed that as the number of cycles increases, a sharp peak in the tangential force is observed to develop towards the end of the sliding stroke (top right and bottom left corners of the fretting loop). Such behaviour has been described by Mulvihill et al. [28] as the effect of interlocking of geometrical features in the contact surfaces, and alternatively described by others [10 & 19] as the ploughing effect as associated with the cylindrical specimen pushing against the edge of the wear scar which is developing on the flat specimen.

This effect is more pronounced as the number of fretting cycles increased due to the wear scar itself becoming deeper; it should be noted that this geometrical change could be associated either with attritive wear or with plastic deformation.. However, it should be noted that the same effect was not observed for fretting test with low value of COF such as in the fretting test of steel in [25]. The loops in low COF fretting tests tend to have flatter parallelogram shapes and no sharp edge peak. The area inside the loops represents the energy dissipated during the fretting motion [13]. The total dissipated energy for every test conditions is calculated by summing up all the fretting loops area for every cycle. Table 2 summarises the value of dissipated energy for each of the tests conducted. As can be seen, the energy dissipated is proportional to the product of the normal applied load and the number of cycles in the case of constant applied displacement.
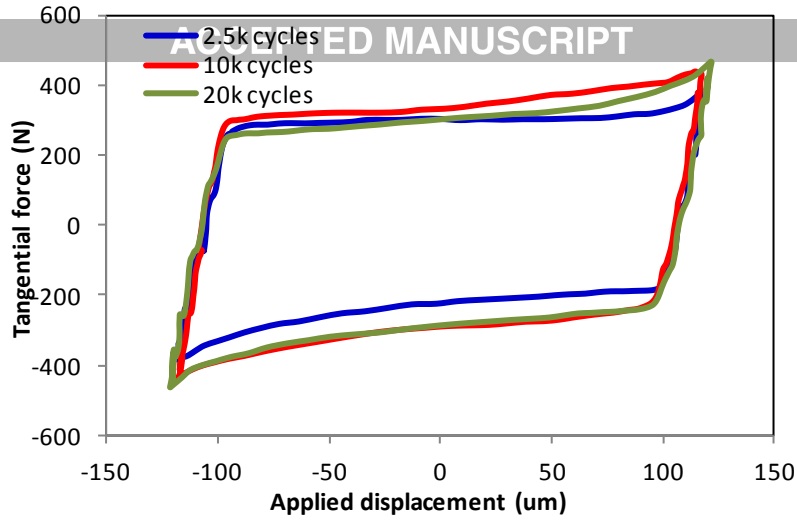

(a)

(b)
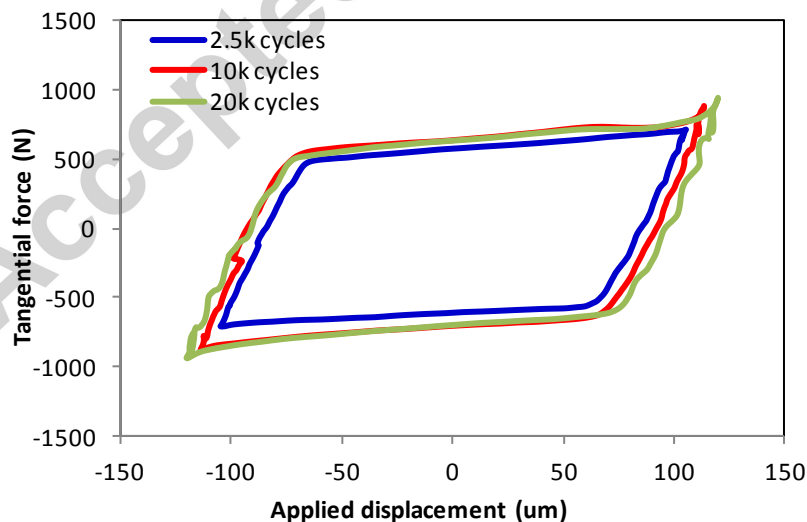
Fig. 6. Typical fretting loops for a) P = 1000 N tests, and b) P = 500 N tests.

Table 2. Total dissipated energy calculated from the fretting loops.

Load (N)	Number of cycles (cycles)	Total dissipated energy (Nm)
1000	1250	245
	2500	582
	5000	1284
	10000	2698
	20000	5605
500	2500	261
	10000	1224
	20000	2587

The maximum coefficient of friction is derived from the maximum value of tangential load observed from the fretting loops divided with the applied normal load. Fig. 7 shows the evolution of the maximum coefficient of friction for the two loading conditions for 2,500, 10,000 and 20,000 cycles. The values of coefficient of friction show repeatability between the two loading conditions and across the three test lengths for each condition. There is a rapid increase in the first 500 fretting cycles due to the vibrator ramping up its displacement from zero to reach the desired applied displacement. The maximum friction then continues to increase from around 0.7 to around 0.9. This increase corresponds to the development of sharp peak edge of the fretting loops due to geometrical wear scar edge ploughing effect as discussed earlier. A similar observation of ploughing effect is also reported by others [10 & 19].

7
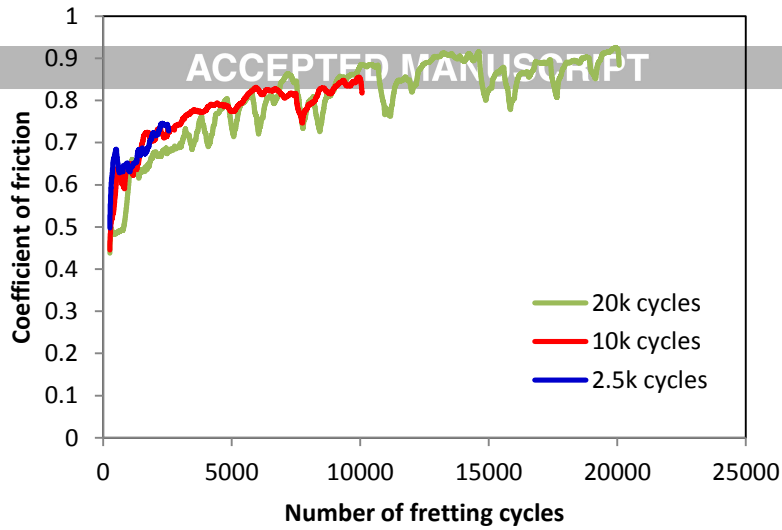
(a)
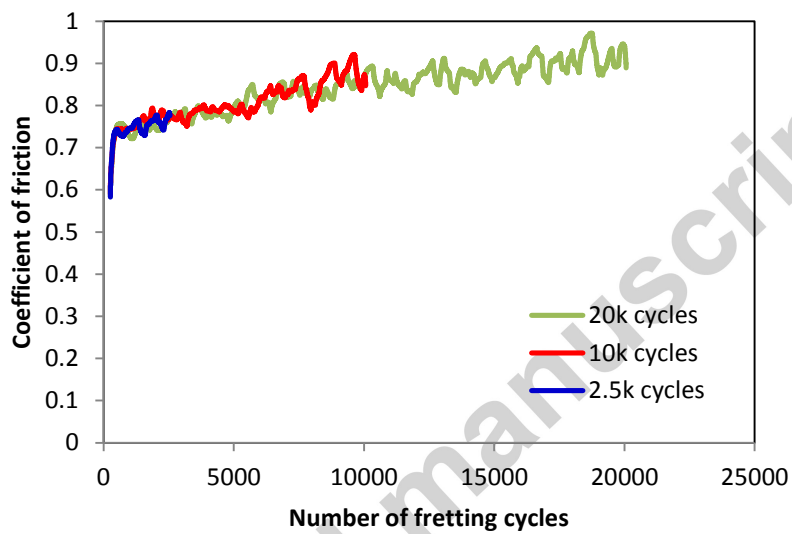
(b)

Fig. 7. Average coefficient of friction evolution with number of fretting cycles for a) $P = 1000$ N tests, and b) $P = 500$ N tests.

Fig. 8 shows the average wear scar profiles for the test conducted at 1000 N and 500 N as a function of number of fretting cycles. Both cases show a wear scar which shape like a *W*-shape scar with the maximum depth and wear scar width increasing with number of fretting cycles. This *W*-shape scar has been commonly reported in the literature for gross sliding fretting tests with high contact friction [10 & 19]. In general, scars from tests conducted under a normal load of 1000 N are deeper and wider compared to those from tests conducted under a normal load of 500 N. For the 500 N tests, the central region of the wear scar is observed to exhibit wear after 2,500 cycles, but then to build back up to the original surface height as the number of cycles increased. In contrast, the central region of the wear scar depth in the test conducted with a 1000 N load continued to increase as the number of cycles increased.

8
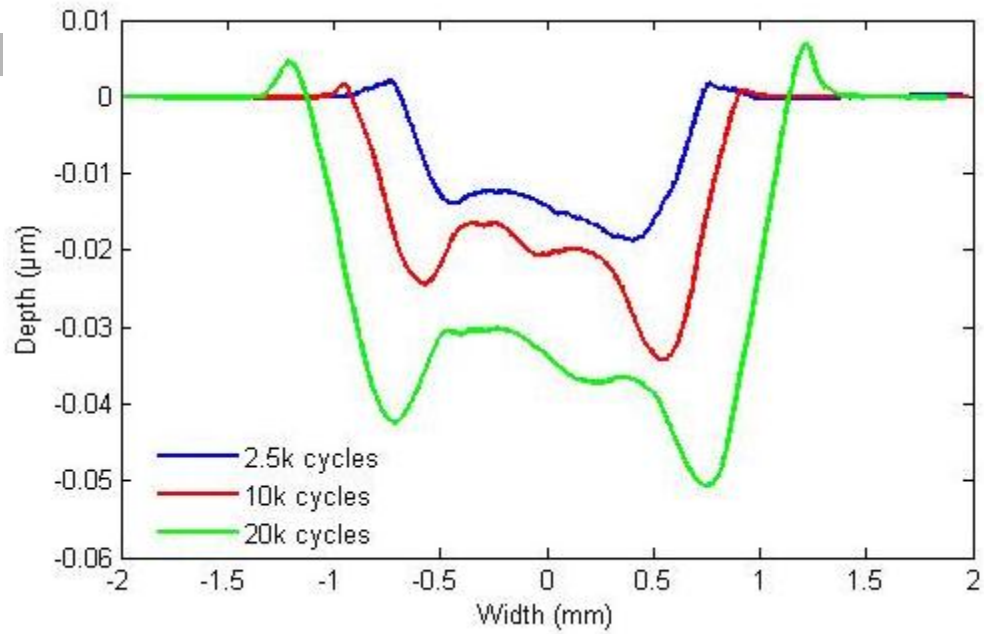
(a)
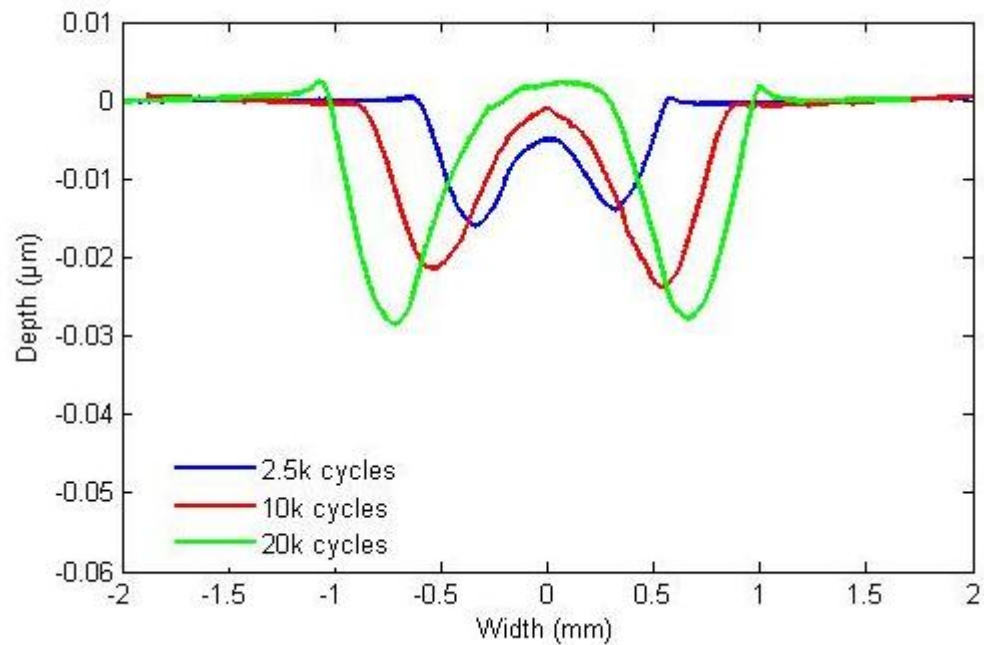
(b)

Fig. 8. Average 2D Surface profiles of the fretting wear scars of the flat specimens at 2,500 cycles, 10,000 cycles, and 20,000 cycles tests for a) $P = 1000$ N, and b) $P = 500$ N..

The wear volume for all wear scars were calculated from the profilometry measurements and plotted against the corresponding dissipated energy for both loading conditions (Fig. 9). It can also be seen that the slope of the curve is reducing with increasing number of cycles, with a higher wear rate being observed at lower total values of energy dissipated. An additional test for 1000 N load case is conducted up to 50,000 cycle (~15,000 total dissipated energy) to confirm the trend of the curve's slope.
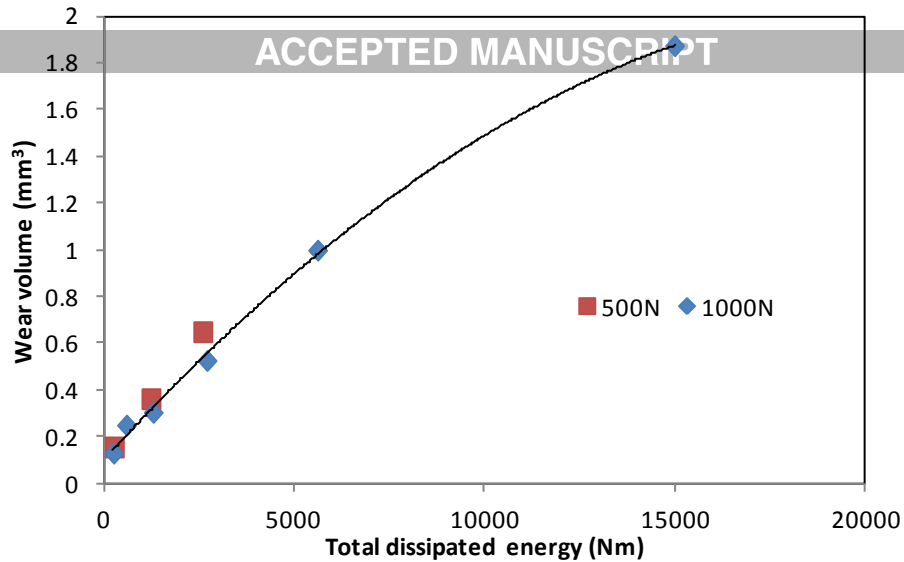
Fig. 9. Plot of total wear volume as a function of the total dissipated energy based on the fretting loops for fretting wear tests conducted with $P = 1000$ N, and $P = 500$ N.

Fig. 10 shows the plan view SEM-BSE images of the wear scar at 2,500, 10,000 and 20,000 cycle's tests. Within the wear scars, the darker regions are associated with oxidised debris; however, there are lighter regions which are associated with titanium-rich regions which have not been oxidised. It can be seen that titanium rich region is developing at the location which correspond to the maximum depth (in reference to Fig. 8a) as the number of cycles increases. It can also be observed that there is a bright region towards the centre of the wear scar suggesting exposed titanium. A higher magnification image of Fig. 10c for the 20,000 cycle test is shown in Fig. 10d. The figure highlighted the sliver features at two locations; i) at the wear scar edge and ii) close to central region. This sliver features correspond to contact geometry hitting the wear scar edge and the central wear scar humps. Similar plan view of the fretting wear scar is observed in 500 N fretting tests (Fig. 11). A pair of exposed titanium regions exists close to the wear scar edge. Sliver features can also be seen but less pronounced on this lower load case.
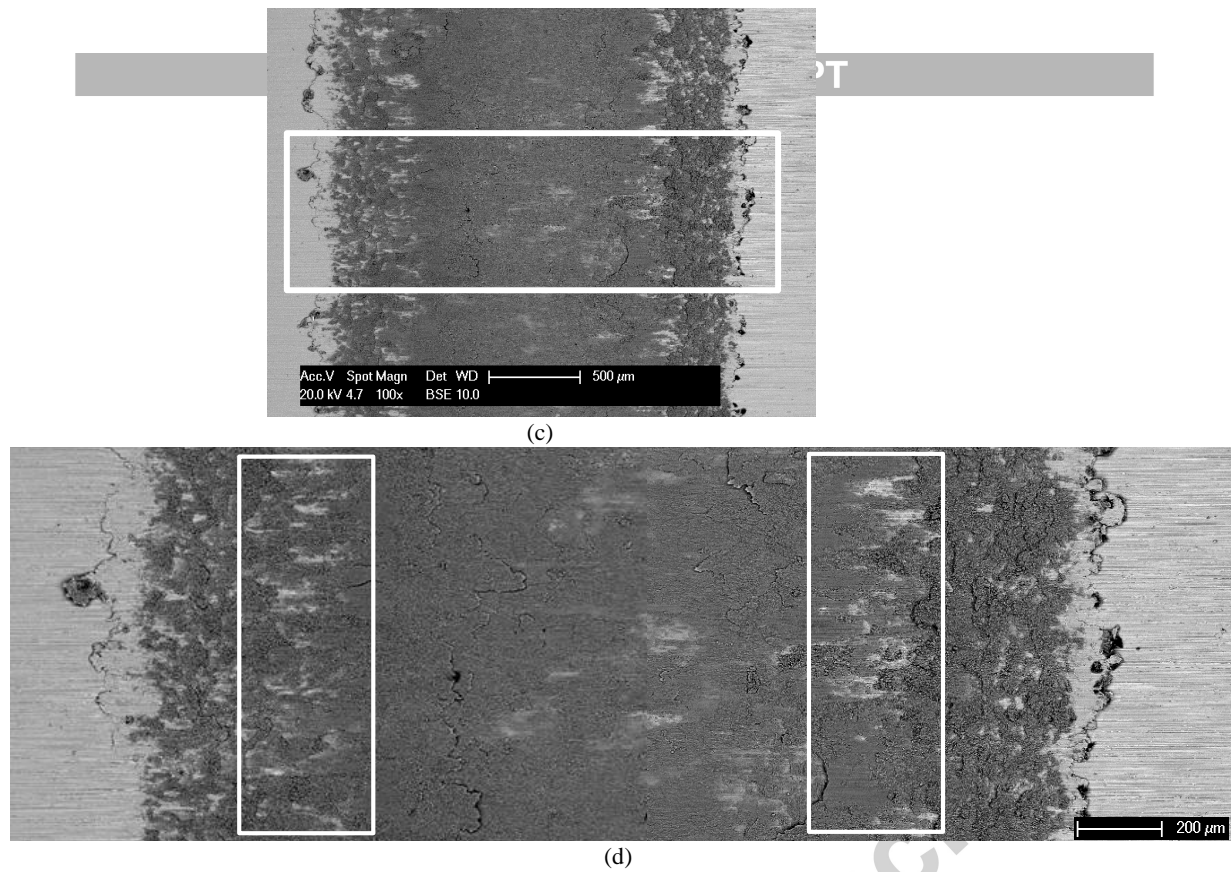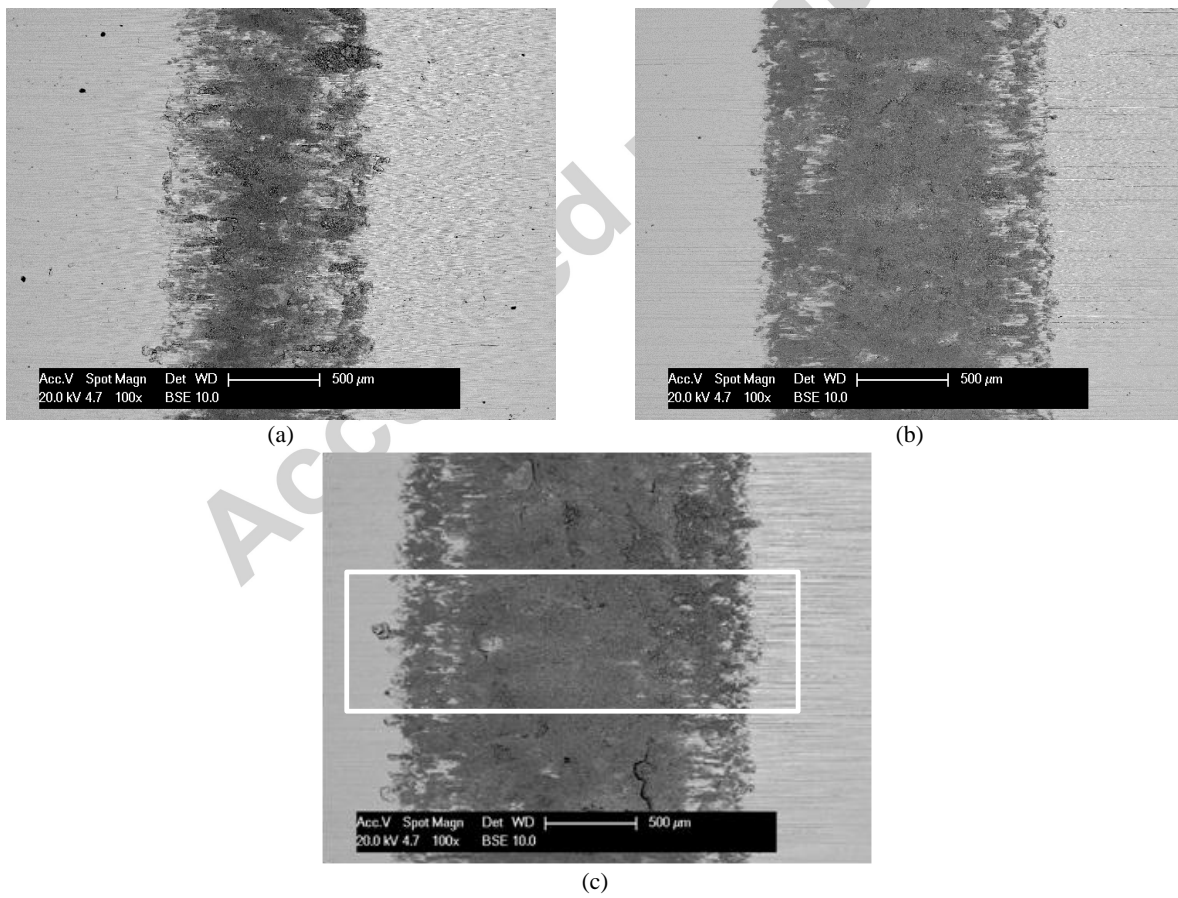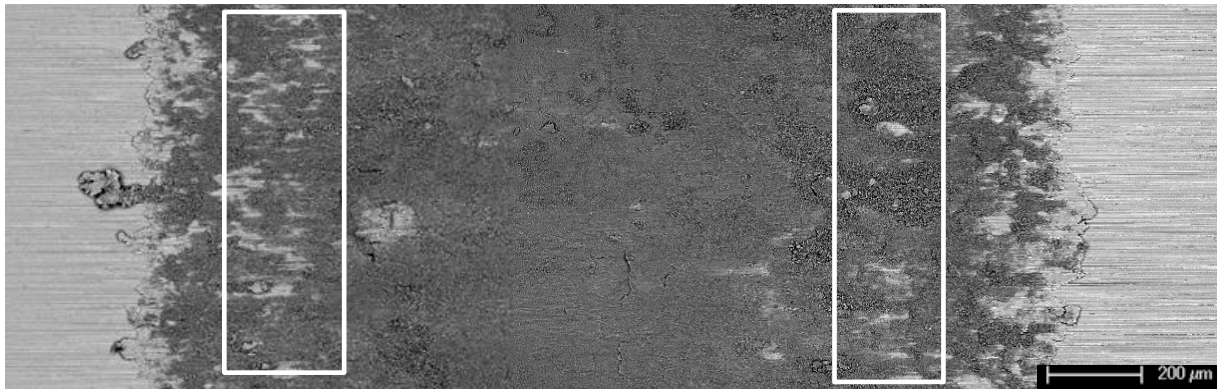

(a)

(b)

(c)

(d)
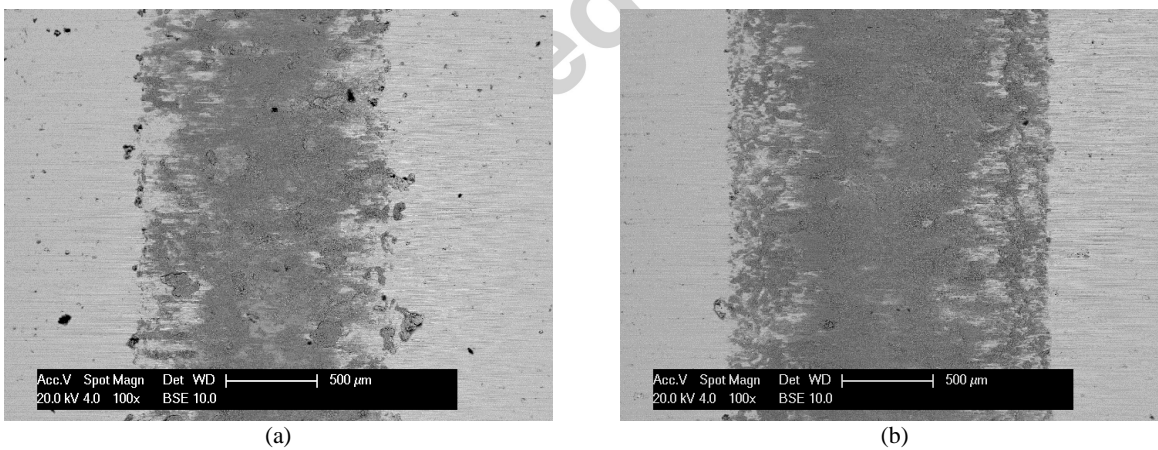
Fig. 10. Plan view SEM-BSE images of the flat specimen wear scar for P = 1000 N, Δ = 120 μm loading conditions for a) 2,500 cycles, b) 10,000 cycles, c) 20,000 cycles tests, and d) 20,000 cycle test at higher magnification (darker regions associated with oxygen rich regions and brighter region associated with titanium rich regions).


(a)

(b)

(c)

(d)

Fig. 11. Plan view SEM-BSE images of the flat specimen wear scar for P = 500 N, Δ = 120 μm loading conditions for a) 2,500 cycles, b) 10,000 cycles, c) 20,000 cycles tests, d) 20,000 cycle test at higher magnification of fig c).

Fig. 12 shows the SEM-BSE cross sectional images for the high load fretting tests following fretting for 2,500, 10,000, and 20,000 cycles. It can be observed that as the number of fretting cycles increased, the *W*-shape wear scar is more pronounced. Corresponding higher magnification images at both the left wear scar edge and at the centre of the wear scar are shown in Figs. 13 and 14 respectively. It can be seen from the images of the wear scar edge (Fig. 13) that as the number of cycles increases, the ploughing effect (as previously described [10 & 19]) becomes more apparent. Plastic deformation can be seen from the evidence of deformation of the microstructural features, particularly evident following 20,000 fretting cycles (Fig. 13c).

In the central region of the wear scar (Fig. 14), it can be seen there is near surface plastic deformation occurring, evidenced from the distorted microstructural features. Following 2,500 cycles, plastically hardened regions can be seen to have formed with micro crack of around 10 μm within these hardened regions (Fig 14a). These regions have had the features of the obliterated α+β microstructure indicating significant plastic deformation. In some part, the plastically hardened material has started to break off from the surface and begun to fracture into coarse particle. Following 10,000 and 20,000 fretting cycles, it can be observed that less plastically hardened regions are observed but mixture of coarse and fine debris (in the form of a debris bed) are now present (Fig 14b & c).
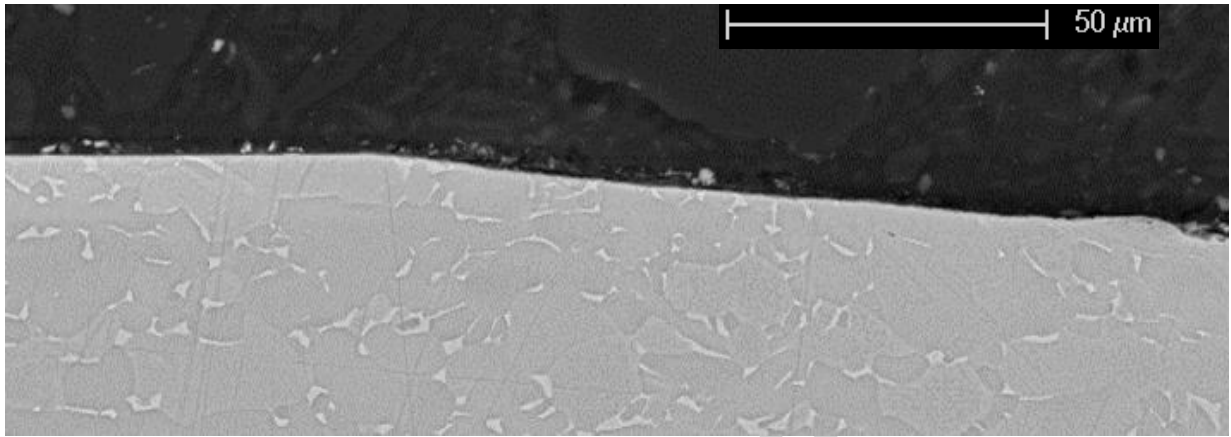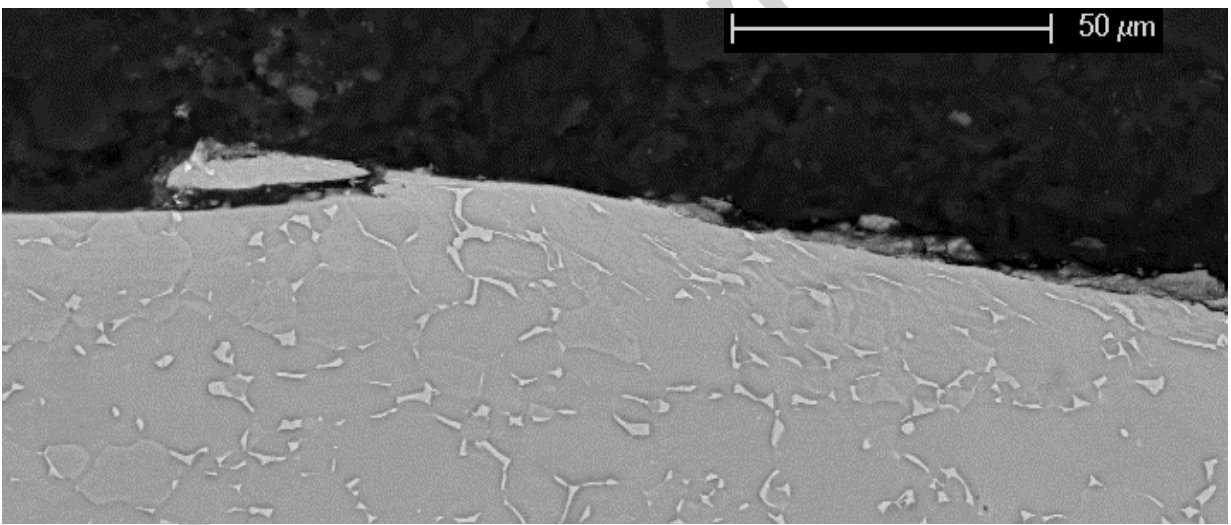

(a)

(b)
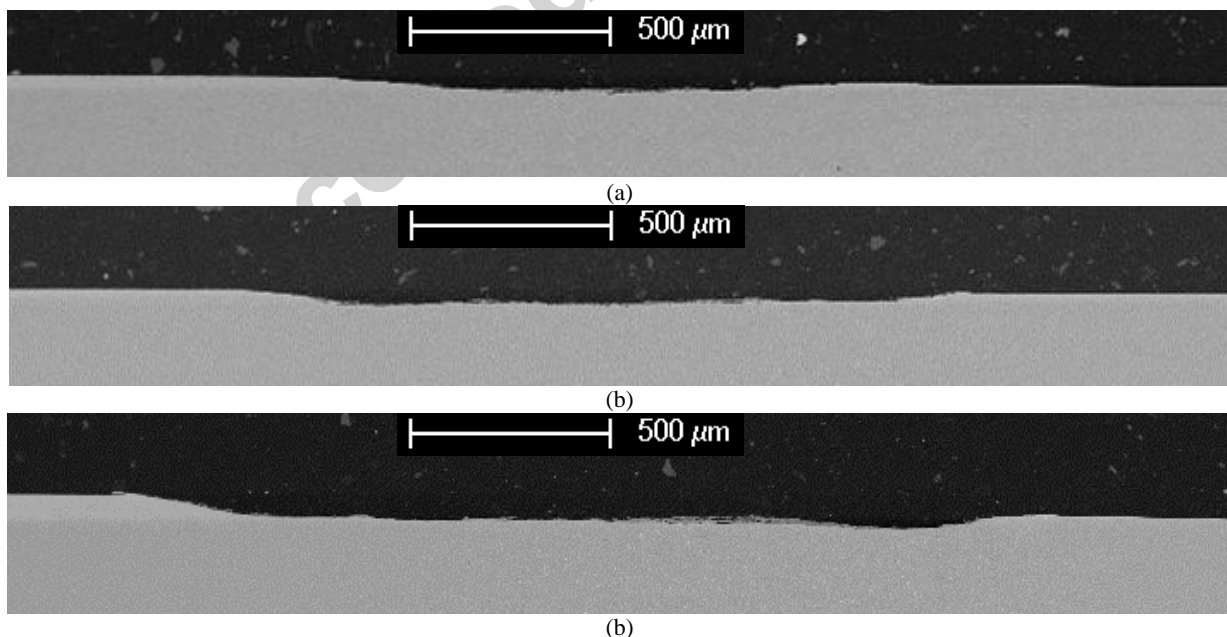
(b)

Fig. 12. SEM-BSE images at 100x magnification for P = 1000 N, Δ = 120 μm loading conditions for a) 2,500, b) 10,000 and c) 20,000 cycles tests.
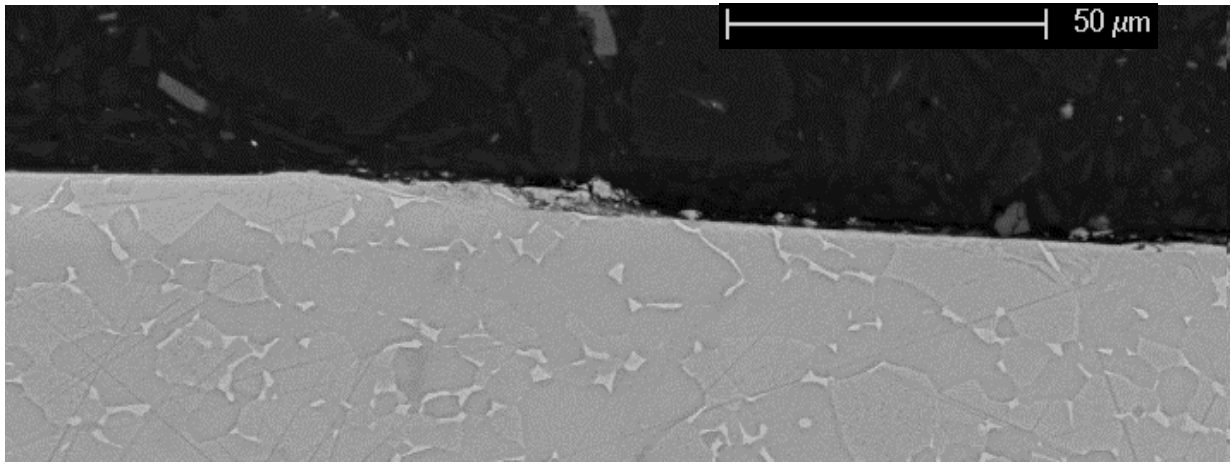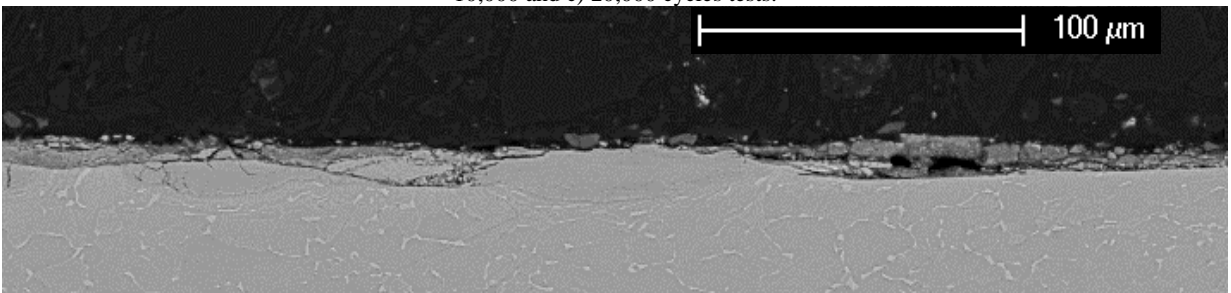
(a)

(b)

(c)

Fig. 13. Left edge wear scar SEM-BSE images at 1600x magnification for $P = 1000$ N, $\Delta = 120$ μm loading conditions for a) 2,500, b) 10,000 and c) 20,000 cycles tests.
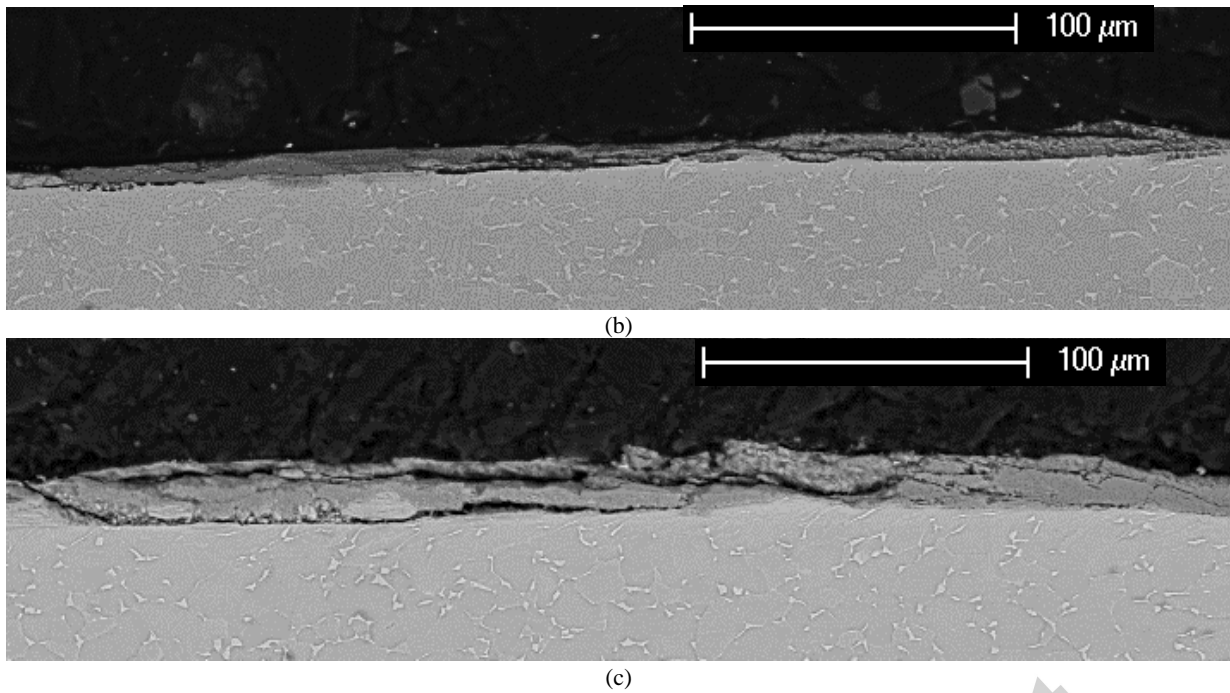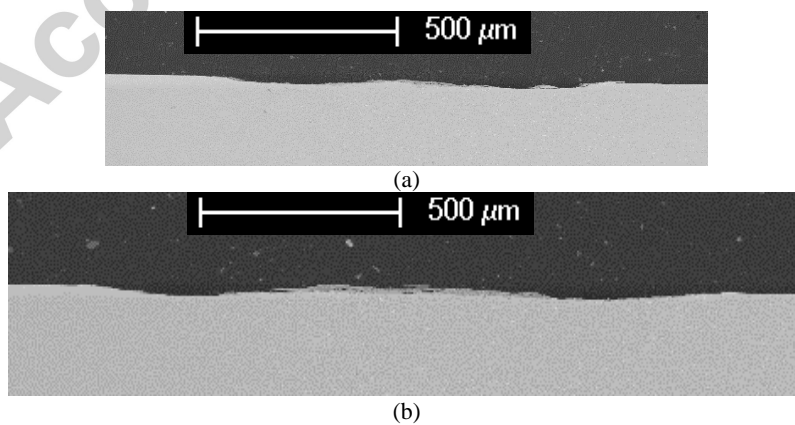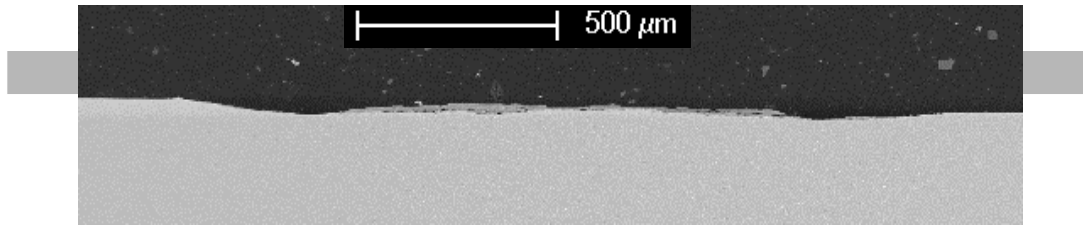

(a)

13

(b)

(c)

Fig. 14. Central region SEM-BSE images at 800x magnification for $P = 1000$ N, $\Delta = 120$ μm loading conditions for a) 2,500, b) 10,000 and c) 20,000 cycles tests.

Fig. 15 shows the SEM-BSE images of flat specimen cross section for the low load case following 2,500, 10,000 and 20,000 cycles. In contrast to high load case in (Fig. 12) the *W*-shape wear scar can be clearly seen for all test durations. It can also be seen that debris is building up in the central region of the wear scar as the number of cycles increase. This is in accord with the profilometry (presented in Fig. 8b) which indicates a build up of material in the central region with an increase in the number of cycles. Higher magnification images of the left wear scar edge are shown in Fig. 16. All cases show plastic deformation as indicated by the deformed microstructural features. As the number of cycles increase, the ploughing effect can be seen to become more significant.

Higher magnification images of the central region wear scar for the low load tests are shown in Fig. 17. Following 2,500 cycles, highly plasticised and severely fragmented subsurface region can be seen (Fig. 17a). Following 10,000 fretting cycles, a debris bed is seen to have formed above the metallic fracture layer and after 20,000 cycles, the debris bed appears to consist of finer debris (Fig. 17b). The SEM images clearly indicate that following 20,000 fretting cycles, and the debris bed consists of a fine outer region, a coarser and more metallic layer comprised of more metallic material, and finally a highly plasticised region which remains part of the substrate (Fig. 17c).

(a)

(b)

14

(c)

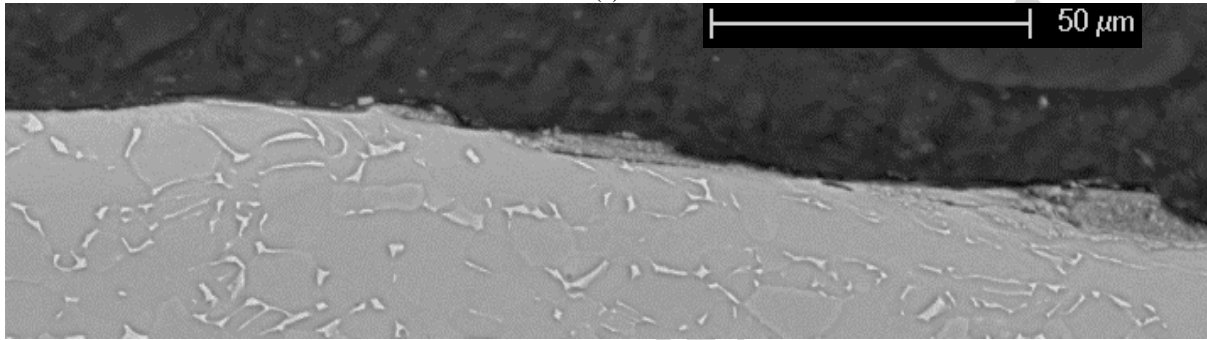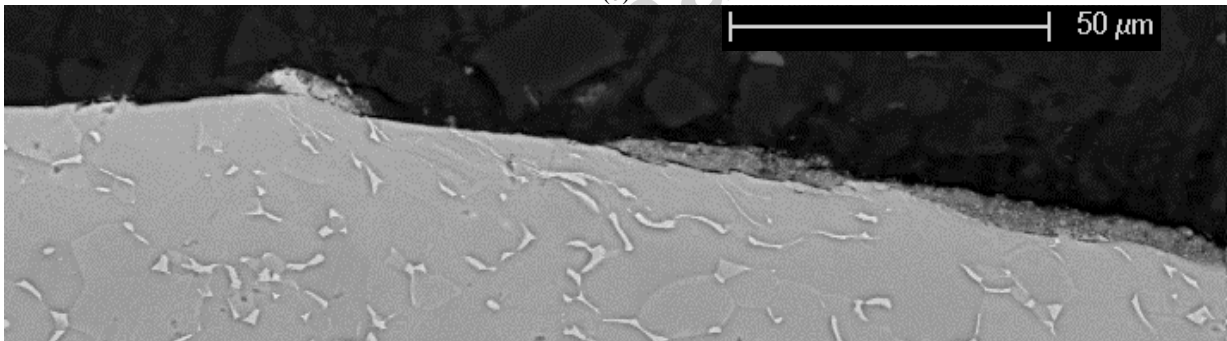Fig. 15. SEM-BSE images, all at the same (low) magnification for $P = 500$ N, $\Delta = 120$ μm loading conditions for a) 2,500 cycles, b) 10,000 cycles, and c) 20,000 cycles tests.
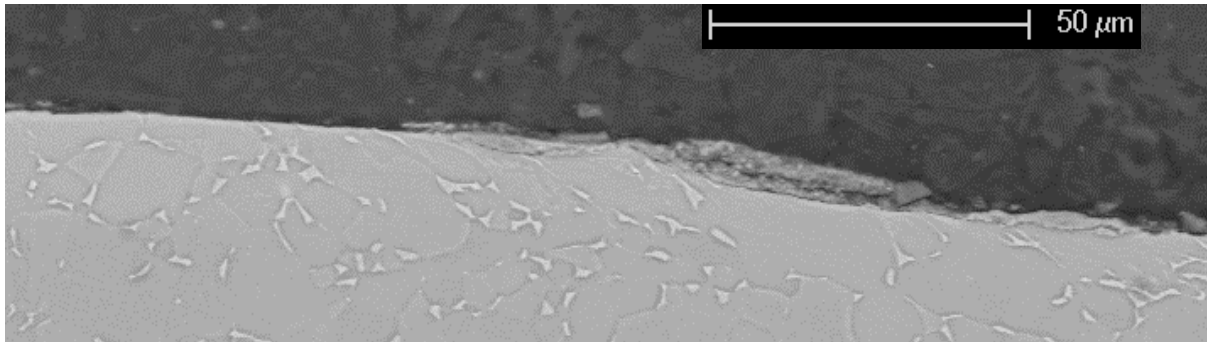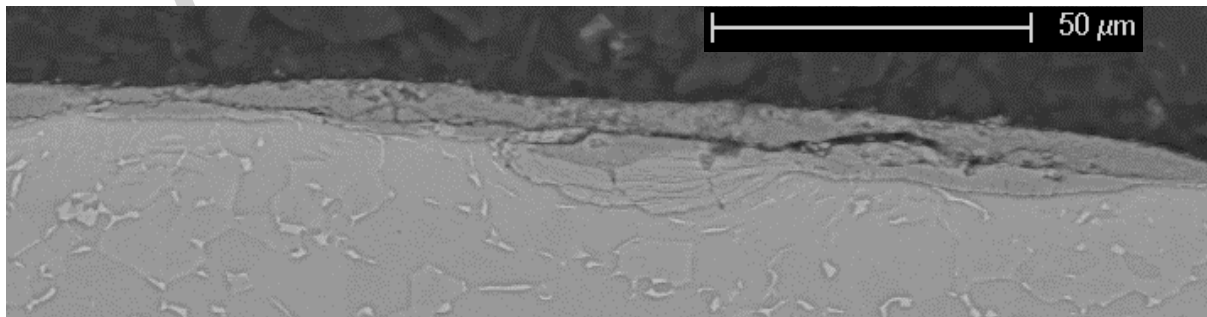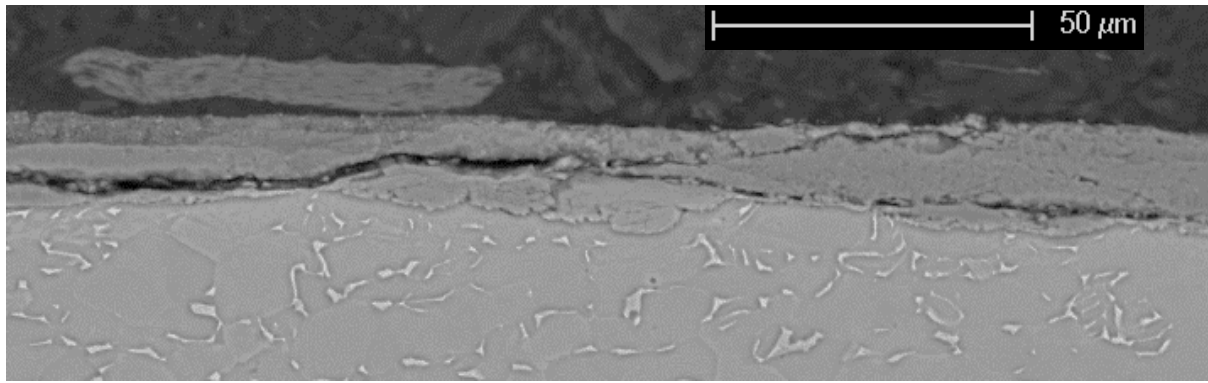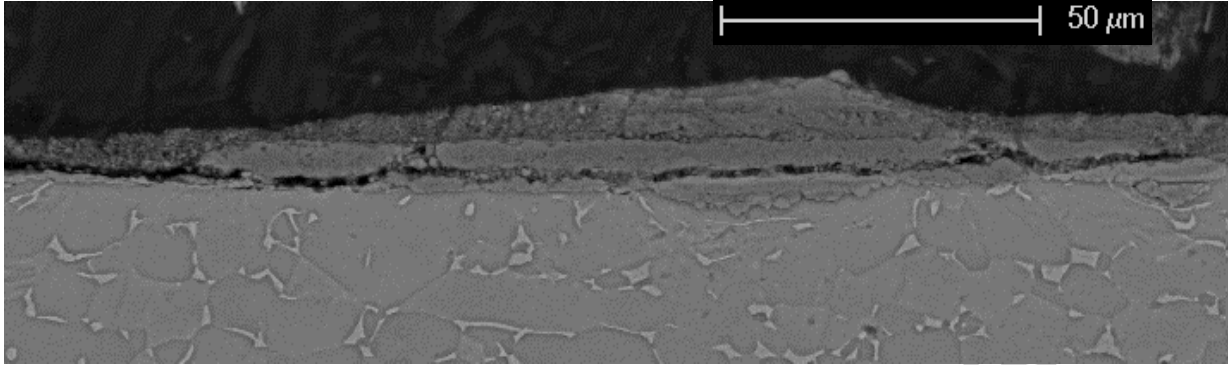

(a)

(b)

(c)

Fig. 16. Left edge wear scar SEM-BSE images at 1600x magnification for $P = 500$ N, $\Delta = 120$ μm loading conditions for a) 2,500 cycles, b) 10,000 cycles, and c) 20,000 cycles tests.

(a)

(b)

(c)

Fig. 17. Central regions-BSE images at 1600x magnification for P = 500 N, Δ = 120 μm loading conditions for a) 2,500 cycles, b) 10,000 cycles, and c) 20,000 cycles tests.

4. Discussion

The evolution of the fretting loops (Fig. 6) and the maximum coefficient of friction (Fig. 7) suggests that gross plastic deformation might occur during the fretting tests. The increasing maximum coefficient of friction with number of cycles is associated with the sharp peak edge observed on the fretting loops as described previously as the ploughing effect [10 & 19]. It is also important to note that the tendency for gross plastic deformation is associated with the high coefficient of friction through the effect of surface shear yielding. This effect is exaggerated by the surface discontinuity generated at the wear scar edge (wear profiles in Fig. 8 and left side wear scar edge cross sectional micrograph in Fig. 13 & 17).

It is proposed that this gross plastic deformation in fretting contributes to the formation of *W*-shape wear scars. Most of the *W*-shape wear scar which have been reported in fretting tests [10, 18, 19, 29 & 30] do have similarity in terms of; i) they exhibit high COF between 0.7 – 0.9; ii) increasing value of COF with increasing number of cycles; and iii) non-horizontal traces in the slipping sections of the fretting loops (i.e. parallelograms with significant increase in load as the slip traverse increases). It is thus proposed that, in fretting with a high frictional contact, severe plastic deformation does occur and contributes to the formation of the *W*-shape wear scar.

Fig. 18 shows the left wear scar edge cross-sectional SEM-BSE image of 1000 N test after 1,250 cycle wear scar. The cross-sectional images show evidence of deep plastic deformation of up to 50 μm depth. Sub-surface deformation can be observed, as indicated by the deformed microstructural features. It can be proposed that based on the plasticity accumulation history, the wear is being generated from plastic hardening turns to metallic fracture, oxidised and becomes wear debris (Fig. 18). It is important to note however the behaviour is different from run in period of wear, since the depth of wear generated is much more than that associated with asperity peaks.
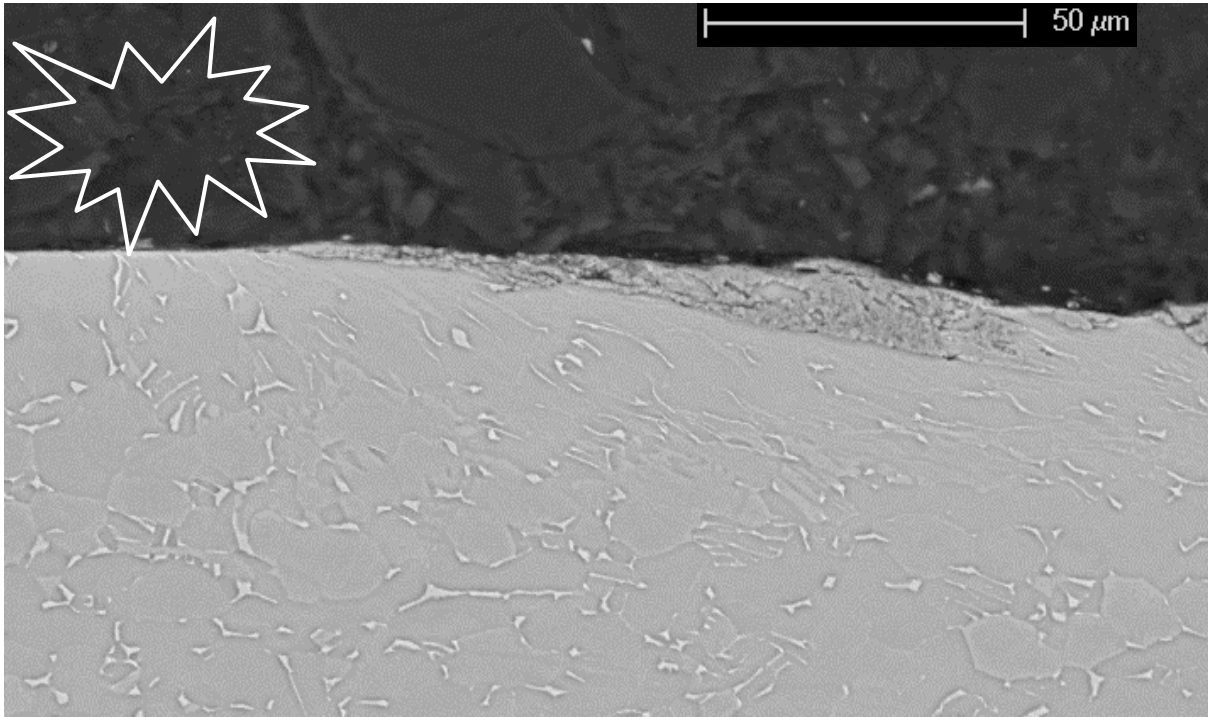
16

Fig. 18. Left edge wear scar SEM-BSE images at 1600x magnification for P = 1000 N, Δ = 120 μm loading conditions for 1,250 cycles tests.

Between them, the high applied normal load and the high tractional load during sliding generates high shear stress causing significant plastic deformation to occur near the surface. As the fretting cycles increase, the plastic strain is accumulated and results in the formation of wear debris in Fig. 18 (close to the contact edge), such a region is observed; debris particles can be observed to be emanating from this damaged region. It is proposed that these regions where plastic deformation is rapidly accumulated lead to significant rates of debris formation and thus to high rates of wear. The wear process itself results in an increase in the conformity of the contact, whereby the contact pressure is reduced (Fig. 19) as predicted by [31] which subsequently lead to a significant reduction in the rate of accumulation of subsurface plastic damage.
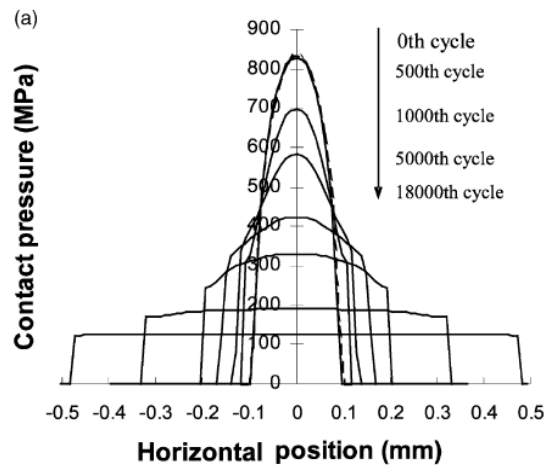
Fig. 19. Finite element prediction of contact pressure distribution evolution with increasing number of fretting cycle in gross sliding condition, after [31].

Plastic deformation will accrue most quickly in contact situations where the pressure is highest, but in all cases, wear will result in a rapid reduction of that contact pressure (as predicted in [31]), whereby the subsurface plasticity may at some point cease to occur. In tests conducted with an applied load of 1000 N, sub-surface plastic strain accumulation will be initially rapid, but this will be less rapid (or perhaps not occur at all) with a lower applied load of 500 N. Given that in both cases, wear will result in a reduction in contact pressure, it is therefore expected that the rate of wear will decrease more rapidly for the

17

tests conducted under an applied load of 1000 N (see Fig. 9) as the sub-surface rate of plastic strain accumulation diminishes and (at some point) ceases to accrue.

This wear scar edge plasticity can be confirmed by the presence of sliver like material on the edge and near the central of the wear scar (due to the *W*-shape of the wear scar causing edge-like effect at the centre peak) as seen from the plan view (Figs. 10d & 11d). The sliver at wear scar edge is more significant on 1000 N load case due to more plasticity for higher load compare to low load (Figs. 13c & 16c). The direction of the sliver being extruded is towards the edge at the wear scar edge and a pair pointing to the centre for the central region. Further it can be seen that the darker region which corresponds to oxide debris is more significant at the region where plasticity accumulation is expected to occur due to edge effect plasticity and brighter region of titanium is located at the valley of wear scar where edge effect plasticity is not observed (comparing Figs. 10d & 11d and Figs. 8a & 8b). The wear scar's central region should have lesser sliver like material at higher cycle due to overall pressure reduction but the edge of the wear scar should have more plasticity generated due to steeper wear scar wall slope which increasing the effect of ploughing.

The effect of high wear rate gross plasticity accumulation can possibly explain the *W*-shape wear scar observed in fretting test conducted by [19, 23]. At low number of cycle, where high magnitude of plastic accumulation at the central region of the wear scar is predicted can cause significant amount of wear (Fig. 20). This will generate initially a *U*-shape wear scar. The next stage is the generation of ploughing effect at the *U*-shape wear scar edge. This cause accumulation of plasticity at the wear scar edge. By assuming the area which having high plasticity accumulation will have higher wear rate than the rest of the contact region, a slightly deeper wear scar is developed at the wear scar edge than non-plasticity accumulated region (Fig. 20). These causes the *W*-shape wear. With further advancement of fretting cycle, the reduced contact pressure (as contact conformity increasing) is not capable of generating edge plasticity thus the *W*-shape is maintained (Fig. 20).
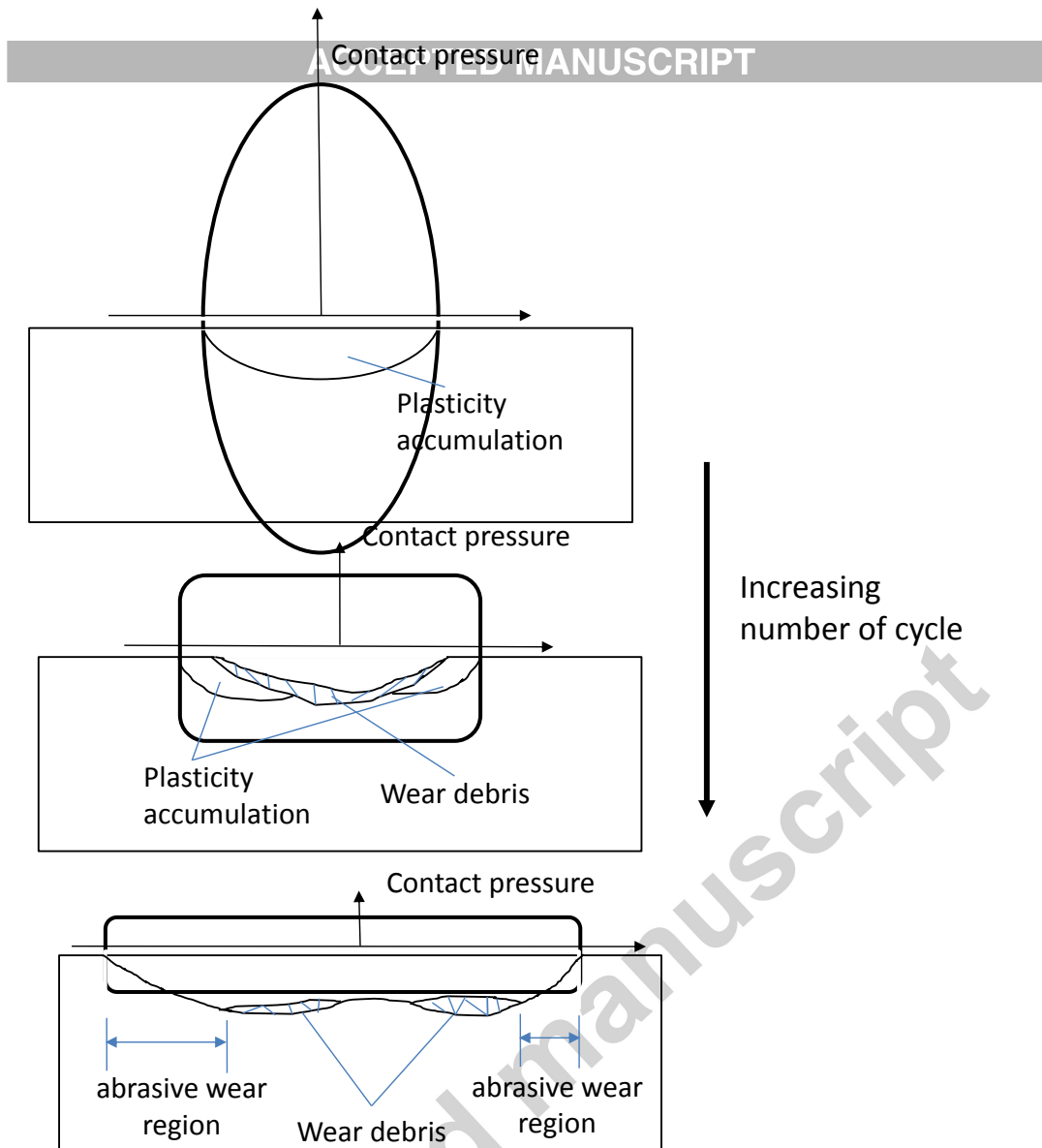
Fig. 20. Schematic view of the plasticity induced wear mechanism with the changes of pressure reduction showing region of plasticity accumulation in gross sliding fretting condition.

This is in agreement with the cross sectional image on the left edge of the wear scar (Figs. 13 & 16) and on the central region cross sectional images (Figs. 14 & 17). At the central region it can also be seen, more plasticity is observed at the early cycle before mixture of debris can be seen at the later stage of wear for both high and low load case. Again this is due to the reduction of pressure which reduces the plastic shearing as wear effects creates conforming contact. This explains the observation by [18] where the central peak region of wear scar is adhesive wear (due to plasticity associated with *W*-shape scar) while the valley of the wear scar is abrasive wear.

Comparing wear profiles of high load and low load case on Fig. 8, difference of wear depth in the central region of wear scar can be seen. High load case produced a significant increase in wear depth at the central region while the low load case shows materials being add up. The reason is significant accumulation of plastic strain accumulated has turn in debris for high load case at the central region. While for the low load case, the plasticity is still in the process of turning into debris. In the low load as the plasticity accumulated is creates metallic fracture which is not compacted material. This is causing the central region to show material build up rather than worn surfaces. The evolution can be clearly seen on Fig. 17 where as the number of cycle increases the plasticity turns into fracturing materials with void gaps between the fractures.

19

Another important point to note is the possibility of different wear rate generated on the contact which might cause the *W*-shape wear scar. As explained earlier there is possibility of high wear rate originated from the plasticity accumulation at the wear scar edge. By looking at the wear profile presented in Fig. 8 for both high and low load case. It can be seen that the valley created in the *W*-shape wear is originated from the wear scar edge from the earlier cycle. To explain this, it can be said that, the *W*-shape wear scar is generated from the edge effect plasticity which promotes higher wear rates compare to other region in the contact.

The overall wear rate however does depend on combined adhesive and abrasive wear mechanism. Abrasive wear and local micro plastic deformations might take place on other contact regions while high localised plasticity occurs at wear scar edge. High load fretting test shows significant plastic deformation (Figs. 13 & 14) but lower wear rate (Fig. 9) while low load test show less plastic deformation (Figs. 16 & 17) but higher wear rate (Fig. 9). Low load case experienced low plastic deformation (i.e. low plasticity induced wear), thus less abrupt pressure reduction causing abrasive type wear dominating the overall wear rate. In contrast for high load case where significant plastic accumulation (i.e. high plasticity induced wear) causing abrupt pressure reduction and low subsequent wear rate (Fig. 9).

In order to understand the evolution of the plasticity induced wear, EDX analysis was carried out on the central wear scar region of the low load case after 20,000 cycle tests. This low load test was selected because the low load will have less rapid plasticity accumulation than the high load case, and thus this will better capture the plasticity induced wear evolution; in addition, the high number of cycles will capture evidence of evolution at different stage of wear, from plasticity accumulation to metallic fracture and oxide debris. Fig. 21 shows the EDX line scan of wear scar in Fig. 17c. The quantitative data from the scan are presented in Fig. 21b for oxygen, titanium, aluminium, and vanadium elements.

Three regions can be identified. It can be seen the oxygen fraction reduces from ~ 70 wt.% to ~ 50 wt.% from the outer debris layer to the inner debris layer, and then down to ~ 40 wt.% as it reaches near-surface plasticity region. It can thus be inferred that the outer layer debris consists of oxide debris whilst the inner debris layer is more metallic in nature. These observations are in accord with the BSE-SEM imaging where oxide debris and metallic debris are seen on the wear surfaces. This observation supports the concept of the plasticity induced wear mechanism in fretting where the wear is generated by the plasticity accumulation before turning into the wear debris.
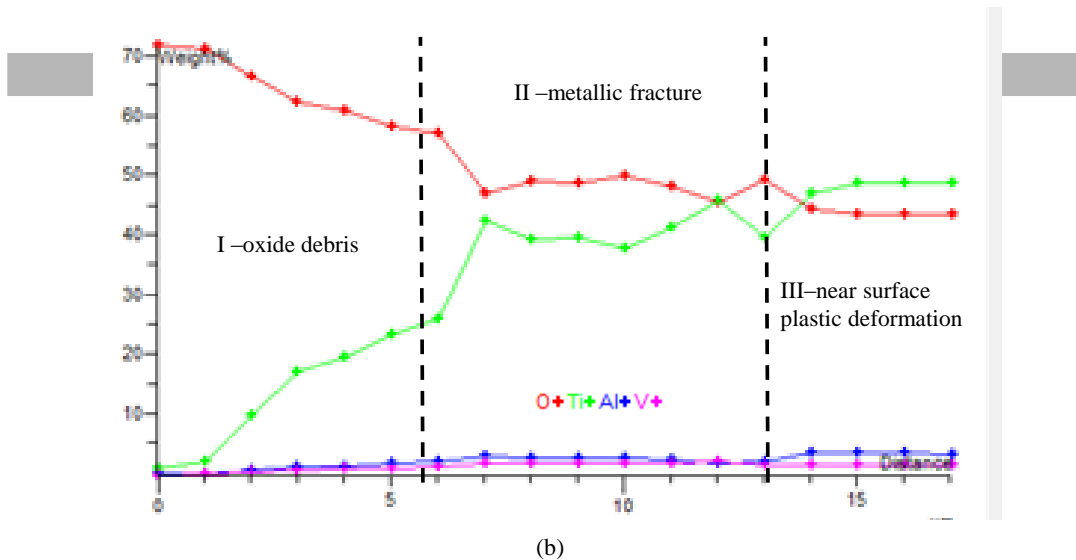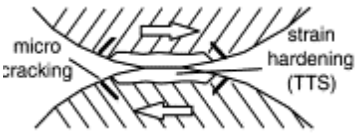

(a)

(b)
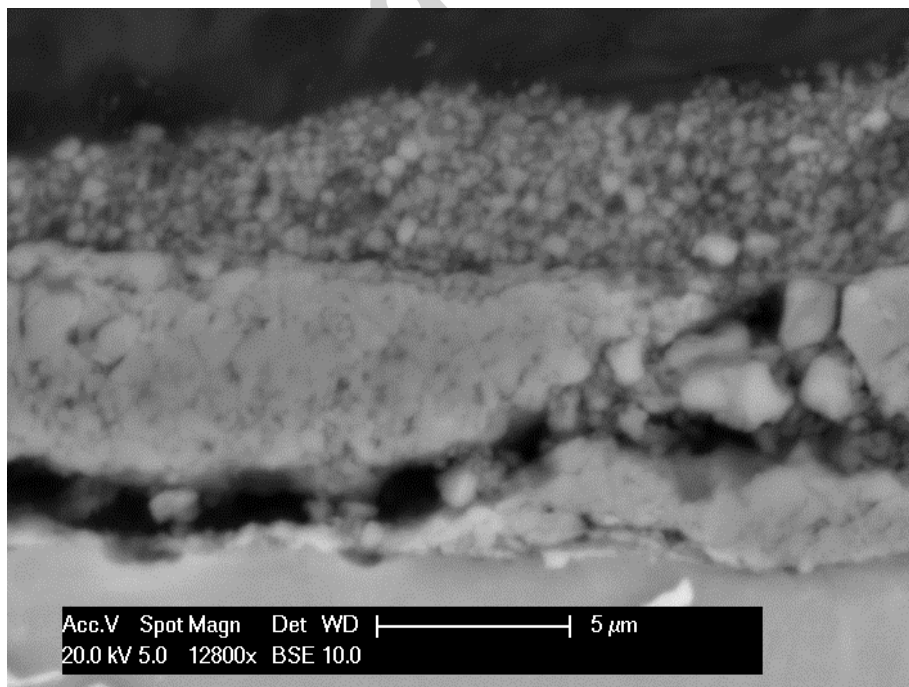
Fig. 21. a) High magnification view of debris region in Fig. 17c showing EDX scan line with difference regions of wear debris, b) relative weightings of the elements along the scan line.

Table 3 summarises current and relevant works conducted by researchers which relate to the plasticity induced mechanism. Similar *W*-shape wear scar have been reported previously in the literature [10, 18, 19, 29 & 30]. They all suggested that there is stage of plasticity accumulation which originated from surface shear yielding and strain hardening. The subsequent stage is the formation of debris through the oxidation process. The damage during the plasticity accumulation stage will cause the material build up from the metallic fracture process. Applied load also plays an important role for the amount of plasticity accumulations and subsequently the wear rate as discussed earlier. High load tends to generate initial high wear rate before the wear rate falls as the plasticity effect becomes less pronounced. For the lower applied load, the edge effect plasticity provides the plasticity accumulations at slower rate.

Archard's wear model has been well accepted to represent the wear rate particularly in reciprocating wear and gross sliding fretting wear. Archard's wear model is mainly assumed an asperity based type wear, while in this case there is a gross plastic deformation which contributes to different type of wear mechanism and subsequently different wear rate. The wear effect depends on the stresses that able to yield the material on the contact surface, the oxidation rate during the TTS formation and abrasive wear mechanism for other contact regions. The general outcome from this study is that on the contact surface of fretting, different wear mechanism might take place depending on the onset of plastic deformation. Plasticity induced wear is expected for plastically deformed surface while Archard's based wear model more suited for non-gross plasticity deformation to represent abrasive wear mechanism.

Table 3. Interpretation of stages of plasticity induced wear mechanism in fretting wear for relatively high contact friction.

Plasticity induced wear mechanism	Plasticity accumulation	Debris formation
Schematic stages	- shear yielding - plasticity accumulation - strain hardening	- TTS formation - oxidation process - oxide debris
Wear mechanism	Material build up - material transfer dominates - distorted microstructural grain	Material removal - coarse/fine oxide debris - loose/compacted debris

21

	• coarse metallic debris	
Load	High loading condition: • gross plasticity at the beginning • high wear rate at the beginning • lower wear rate for subsequent wear	Low loading condition: • edge effect plasticity • small amount of plastic accumulation • slow wear process and debris generation • less dramatic saturation
Number of cycles	Low number of cycle: • plasticity still accumulating not sufficient to turn in oxide debris • metallic fracturing	High number of cycles: • accumulated plasticity has turns into oxide debris

5. Conclusions

This study was conducted to investigate the evidence of plasticity induced wear mechanism in gross sliding fretting tests of a non-conforming Ti-6Al-4V contact with friction coefficient of 0.7 to 0.9. Two loading conditions were chosen to portray high load and low load conditions. The tests were conducted from low number of cycles of 1,250 to 20,000 cycles to capture the evolution of the plastic deformation and debris generation during the tests. The followings conclusions can be deduced from the study:

- Fretting condition with gross surface plastic deformation will normally occur for high contact friction case and evidence of increasing COF with number of cycle and fretting loops with sharp peak edge can be observed in all cases. The plasticity is mainly generated by the edges of the wear scar.

- The accumulation of the plasticity over number of cycles will cause a plasticity induced wear mechanism through the evolution of metallic fracture and oxidation process of the debris.

- High loads will generate more plastic deformation and subsequent high wear rate at the early fretting cycle, but lower wear rate later on the cycle compare to low load case.

- As the wear volume increases and the contact becomes conforming, the near surface plastic deformation causes a reduction of the wear rate.

- The interpretation of the wear mechanism of the fretting surfaces should consider the deformation regime in the contact region. Different wear rate associated with plastic deformation in the contact might promote the *W*-shape wear scar in gross sliding fretting.

- The authors emphasize that the presented conclusions only apply to the gross sliding fretting of the Ti-6Al-4V alloy. Further research should be conducted with other materials for generalisation.

References

[1] Kim, D.-G.& Lee, Y.-Z. (2001) Experimental investigation on sliding and fretting wear of steam generator tube materials. Wear, 250, 673-680.

[2] Bozdana, A.T. (2005) On the mechanical surface enhancement techniques in aerospace industry - a review of technology. Aircraft Engineering and Aerospace Technology, 77, 279-292.

[3] Leen, S. B., Hyde, T. H., Ratsimba, C. H. H., Williams, E. J. &Mccoll, I. R. (2002) An investigation of the fatigue and fretting performance of a representative aero-engine spline coupling. Journal of Strain Analysis for Engineering Design, 37, 565-583.

[4] Varenberg, M., Etsion, I. &Halperin, G. (2004) Slip index: a new unified approach to fretting. Tribology Letters, 17, 569-573.

[5] Mindlin, R. D. (1949) Compliance of elastic bodies in contact, Journal of Applied Mechanics-Transactions of the ASME, 16 (3), 259-268.

[6] Cattaneo, C. (1938) Sulcontatto di due corpielastici: distribuzion locale deglisforzi, Reconditi dell Academia nazionaledeiLincei 27, 342-348, 434-436, 474-478.

[7] Johnson, K. L. (1985) Contact Mechanics, Cambridge University Press, Cambridge.

[8] Collin, J.A. & Macro, S.M. (1964) Effect of stress direction during fretting on subsequent fatigue life, Proceeding American Society for Testing and Materials 64, 547-560.

[9] Dobromirski, J.M. (1992) Variable of fretting process: are there 50 of them?, Standardization of fretting fatigue test methods and equipment, Attia/Waterhouse, ASM STP, Philadelphia.

[10] Fouvry, S., Duó, P. & Perruchaut, P. (2004) A quantitative approach of Ti-6Al-4V fretting damage: friction, wear and crack nucleation. Wear, 257, 916-929.

[11] Vincent, L.,Berthier,Y. & Godet, M.(1992) Testing Methods in Fretting Fatigue: A critical appraisal, ASTM STP, 1159, 33–48.

[12] Vingsbo, O. & Soderberg, S. (1988) On Fretting Maps. Wear, 126, 131-147.

[13] Fouvry, S. & Kapsa, P. (2001) An energy description of hard coating wear mechanisms. Surface and Coatings Technology, 138, 141-148.

[14] Archard, J. F. (1953) Contact and rubbing of flat surfaces. Journal of Applied Physics 24, 981-988.

[15] Archard, J. F. &Hirst, W. (1956) Wear of metals under unlubricated conditions. Proceedings of the Royal Society. A, 236, 763-775.

[16] Fouvry, S., Kapsa, P., Zahouani, H. & Vincent, L. (1997) Wear analysis in fretting of hard coatings through a dissipated energy concept. Wear, 203-204, 393-403.

[17] Heredia, S. & Fouvry, S. (2010) Introduction of a new sliding regime criterion to quantify partial, mixed and gross slip fretting regimes: Correlation with wear and cracking processes. Wear, 269 (7-8), 515-524.

[18] Magaziner, R. S., Jain, V. K. & Mall, S. (2008) Wear characterization of Ti-6Al-4V under fretting-reciprocating sliding conditions. Wear, 264, 1002-1014.

[19] Mohd Tobi, A. L., Ding, J., Bandak, G., Leen, S. B. & Shipway, P. H. (2009) A study on the interaction between fretting wear and cyclic plasticity for Ti-6Al-4V. Wear, 267, 270-282.

[20] Fouvry, S., Kapsa, P., & Vincent, L. (2001) An elastic–plastic shakedown analysis of fretting wear, Wear, 247 (1) 41–54.

[21] Paulin, C., Fouvry, S., & Meunier, C. (2008). Finite element modelling of fretting wear surface evolution: Application to a Ti-6A1–4V contact. Wear, 264 (1-2), 26-36.

[22] Warmuth A.R., Shipway P.H., Sun W. (2015). Fretting wear mapping: the influence of contact geometry and frequency on debris formation and ejection for a steel-on-steel pair. RSPA Proceedings A. 471, 1-22.

[23] Hurricks, P. L. (1970) The mechanism of fretting wear – A review, Wear 15, 389-409.

[24] Sauger, E., Ponsonnet, L., Martin, J.M., Vincent, L. (2000) Study of the tribologically transformed structure created during fretting tests. Tribology International, 33 (11), 743-750.

[25] Mohd Tobi, A. L. (2010) Modelling of the fretting wear of a coated substrate. PhD Thesis, University of Nottingham.

[26] Kapoor, A. (1997) Wear by plastic ratchetting. Wear, 212, 119-130.

[27] Everitt, N. M., Ding, J., Bandak, G., Shipway, P. H., Leen, S. B. & Williams, E. J. (2009) Characterisation of fretting-induced wear debris for Ti-6Al-4 V. Wear, 267, 283-291.

[28] Mulvihill, D. M., Kartal, M. E., Nowell, D., Hills, D. A., (2011) Investigation of the Friction Variation with Sliding which is Commonly Observed in Individual Fretting Test Cycles. Applied Mechanics and Materials, 70, 213-218.

[29] Jin, O. & Mall, S. (2002) Effects of independent pad displacement on fretting fatigue behavior of Ti–6Al–4V. Wear, 253, 585-596.

[30] van Peteghem, B., Fouvry, S., & Petit, J. (2011) Effect of variable normal force and frequency on fretting wear response of Ti–6Al–4V contact. Wear, 271, 1535-1542.

[31] Ding, J., Leen, S. B. & McColl, I. R. (2004) The effect of slip regime on fretting wear-induced stress evolution. Int. J. Fatigue, 26, 521-531.

Highlights

- Plasticity based wear mechanism in the fretting wear of Ti-6Al-4V
- The evolution of fretting wear rate associated with changes of wear mechanisms.
- Different interpretation of wear rate on different area of contact due to plastic deformation.